Title

Photoinduced Carrier Generation and Distribution in Solution-Deposited Titanyl Phthalocyanine Monolayers

Permalink

https://escholarship.org/uc/item/19k3q4mm

Authors

Wang, Shenkai
Chiang, Naihao
Guo, Han
et al.

Peer reviewed

Photoinduced Carrier Distribution in Titanyl Phthalocyanine Monolayers

Shenkai Wang,[†,‡] Naihao Chiang,[†,‡] Han Guo,[†,‡] Natcha Wattanatorn,[†,‡] Kristopher Barr,[†,‡] Philippe Sautet,[†,§] Anastassia N. Alexandrova,[†,‡*] and Paul S. Weiss[†,‡,⊥,*]

[†]Department of Chemistry and Biochemistry, University of California, Los Angeles, Los Angeles, California 90095, United States

[‡]California NanoSystems Institute, University of California, Los Angeles, Los Angeles, California 90095, United States

[§]Department of Chemical and Biomolecular Engineering, University of California, Los Angeles, Los Angeles, California 90095, United States

[⊥]Department of Materials Science and Engineering, University of California, Los Angeles, Los Angeles, California 90095, United States

1

ABSTRACT: We prepared titanyl phthalocyanine (TiOPc) monolayers on sapphire-prism supported Au{111} substrates through solution deposition and characterized their photo-responses using a custom-built laser-assisted scanning tunneling microscope under ambient conditions. Two types of lattice structures (hexagonal and rectangular) were observed and the distributions of photo-induced charges were measured under evanescently introduced 633 nm and 780 nm laser illumination. The distributions of photoelectrons in molecules in hexagonal lattices match theoretically calculated charge density changes in TiOPc molecules upon excitation. However, the photo-responses of TiOPc molecules in rectangular lattices are different than those predicted and TiOPc molecules in these arrangements may have lower excitation probabilities at 633 nm and 780 nm. Our results suggest that the photo carrier generation efficiency of TiOPc molecules is related to their packing arrangements in monolayers and local environments.

KEYWORDS: titanyl phthalocyanine, laser-assisted scanning tunneling microscopy, density functional theory, molecular orbitals, single molecule absorption

TOC: Still working on it.

2

Titanyl phthalocyanine (TiOPc, Figure 1a) has been widely studied as a potential candidate for organic photovoltaic solar cells,[1-6] organic light emitting diodes,[7] and field effect transistors[8-10] due to its efficient photoelectric activities in the visible and near-IR regions.[11] Titanyl phthalocyanine is a nonplanar molecule with the titanyl group located perpendicular to the phthalocyanine plane (Figure 1a), resulting in various crystal structures. Three major polymorphs have been reported for TiOPc, including monoclinic phases I (β-TiOPc) and Y, and a triclinic phase II (α-TiOPc).[12] The optical responses of different TiOPc polymorphs are significantly different from each other since their carrier generation efficiencies greatly depend on intermolecular interactions.[3,4,12] Understanding the relationships between the arrangements of the TiOPc molecules and their photoelectric properties is critical for optimizing the performance of TiOPc based optoelectronic devices. More generally, optimizing the structures and relative orientations of components of solar cells and other energy harvesting devices has the potential to increase the efficiencies of photoexcitation, charge separation, and the overall ~~devices~~device performance. Thus, as a community, we have developed new multimodal nanoscale analysis tools that enable us to elucidate structures while simultaneously measuring local spectra and function.[13-25]
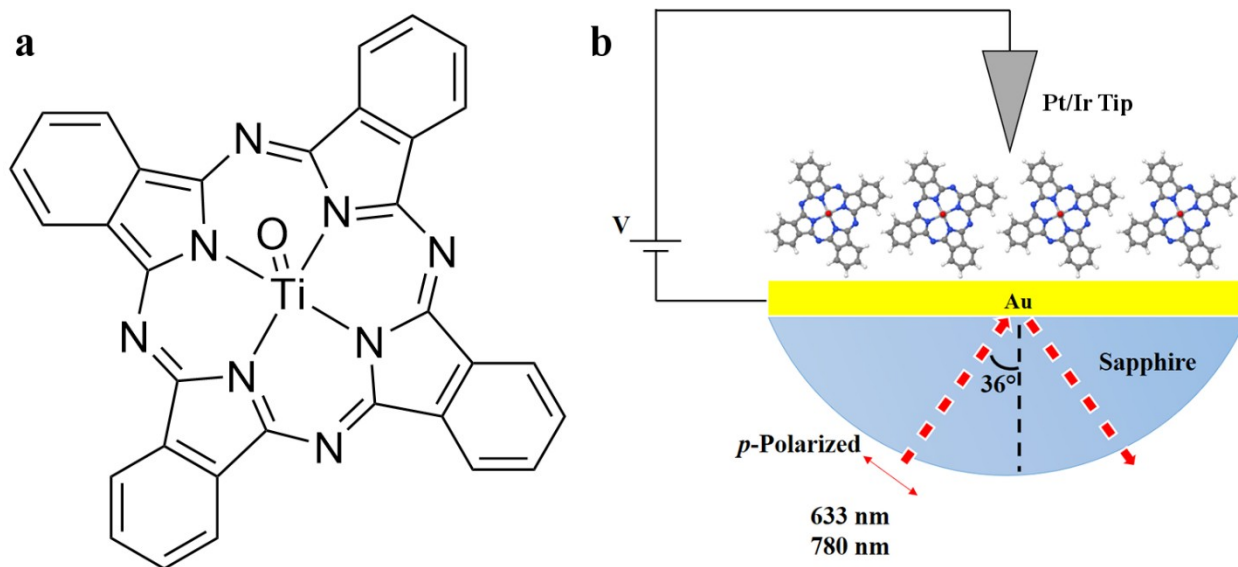
Figure 1. (a) Chemical structure of titanyl phthalocyanine (TiOPc). (b) Schematic illustration of TiOPc monolayers photoexcited evanescently and studied by laser-assisted scanning tunneling microscopy.

Scanning tunneling microscopy (STM) has been used to study the adsorption of TiOPc molecules on various surfaces.[10,26-32] In most of these studies, the deposition of TiOPc molecules was conducted in ultra-high vacuum (UHV) and therefore the arrangements of the molecules are significantly different from TiOPc crystals. When approaching low surface coverages (*i.e.*, < 1 monolayer), TiOPc molecules adsorb on metal surfaces with their phthalocyanine plane parallel to the substrates.[32] In monolayers prepared *in vacuo*, TiOPc molecules are distorted and their arrangements depends strongly on the structure of the substrates.[10,27-31]

Incorporating laser irradiation into the tunneling junction extends the capabilities of STM and enables us to probe photoinduced carrier dynamics at the nanoscale.[14,16,18,33-37] The photo excited orbitals of a variety of

photoactive nanostructures and molecules have been visualized with submolecular resolution and studied by local spectroscopic methods.[38-45] Here, we used a custom-built laser-assisted STM[23,25] to measure the photo-responses of TiOPc monolayers that were prepared through solution deposition,[26,46] to reproduce real-life applications more realistically. We observed two types of lattice structures, which are different from those reported for UHV deposition or at liquid/solid interfaces. The lattice parameters we observed are different from bulk TiOPc crystals but the molecules are densely packed in both lattices. Three lasers with wavelengths of 405 nm, 633nm, and 780 nm were used for interrogating the optical responses of TiOPc molecules in monolayers. Both 633 nm and 780 nm falls in the Q band of TiOPc, and 405 nm laser was used in a control experiment to test the thermal expansion effect of the STM tip-sample junction since TiOPc does not absorb 405 nm light efficiently.[12] The laser beams were modulated by a chopper wheel at 4.8 kHz and were introduced into the tunneling junction through total internal reflection, as illustrated in Figure 1b. The chopper wheel creates a reference frequency input to a lock-in amplifier for phase-sensitive detection, so that light-triggered changes in tunneling current can be recorded and spatially resolved. Different photo-responses were observed for the two lattice structures. Density functional theory (DFT) calculations of the ground state and excited state molecular orbitals were compared to and used to interpret the data. Our results indicate that the

photoinduced carrier generation within TiOPc monolayers depends on the arrangement of TiOPc molecules and local environment.

Results and Discussion

We prepared TiOPc monolayers by immersing freshly flame-annealed sapphire-prism-supported Au{111} substrates in saturated TiOPc ethanolic solution for 10 min. The substrates were then cleaned with ethanol and characterized with laser-assisted STM. We observed two types of lattice structures in TiOPc monolayers. The first lattice has unit cell parameters a = 1.21 ± 0.02 nm, b = 0.64 ± 0.01 nm, and α = 123 ± 1° (Figure 2a). The unit cell parameters for the second structure are c = 1.18 ± 0.02 nm, d = 0.40 ± 0.01 nm, and β = 89 ± 3° (Figure 2b). We tentatively name these structures hexagonal and rectangular lattices, respectively. The unit cell parameters reported here suggest that in the observed monolayers, TiOPc molecules are densely packed and stand nearly normal to the Au{111} surface, so the interactions between the molecules and the substrates should be weak. Therefore, in DFT calculations, we neglected the effects of the surface-molecule interactions and all calculations ~~on the geometry optimization for TiOPc molecules and the band-decomposed charge density~~ were performed for gas-phase TiOPc molecules assembled in monolayers, with the periodic boundary conditions applied. The electron density of the highest occupied molecular orbital (HOMO) of TiOPc is shown in Figure 3a, and the proposed packing arrangements for hexagonal and rectangular lattices are shown in Figure 3b,c, respectively. Our calculations also indicate

6

that minimal strain energies are achieved for both hexagonal and rectangular lattices when TiOPc molecules are tilted about 20° from the surface normal (see supporting information). The intermolecular distances in the hexagonal and rectangular lattices are close to those reported in TiOPc crystals and liquid/solid interface[11,12,26] and are significantly smaller than those previously reported for STM data in UHV.[27-29,32]
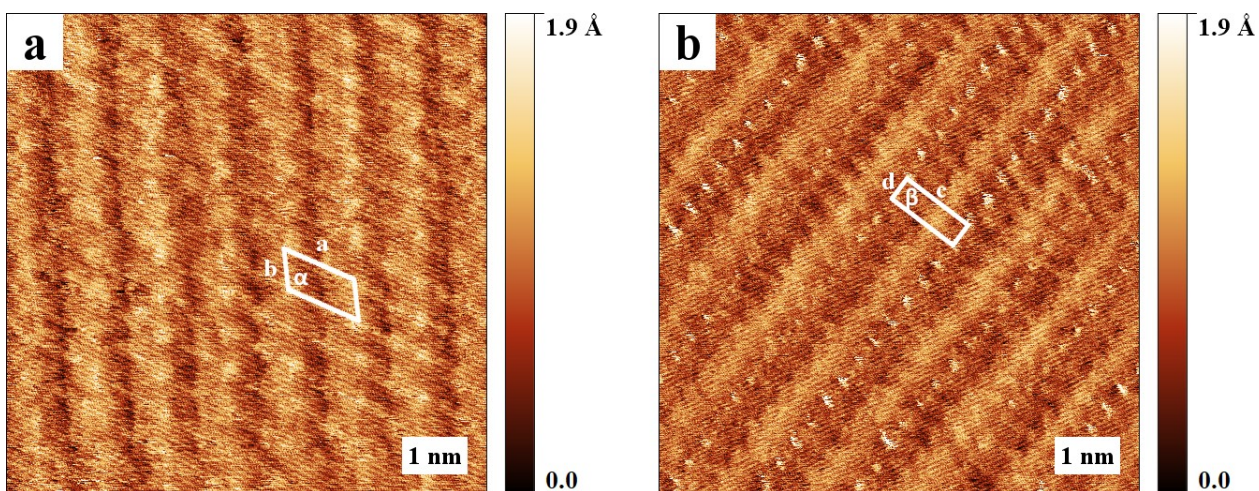
Figure 2. Scanning tunneling microscopy (STM) images of titanyl phthalocyanine (TiOPc) monolayers on Au{111}. (a) Hexagonal lattice. Unit cell parameters are a = 1.21 ± 0.02 nm, b = 0.64 ± 0.01 nm, α = 123 ± 1°. (b) Rectangular lattice. Unit cell parameters are c = 1.18 ± 0.02 nm, d = 0.40 ± 0.01 nm, β = 89 ± 3°. All images were collected at a sample bias of −1.00 V and a tunneling current of 70.0 pA.

7
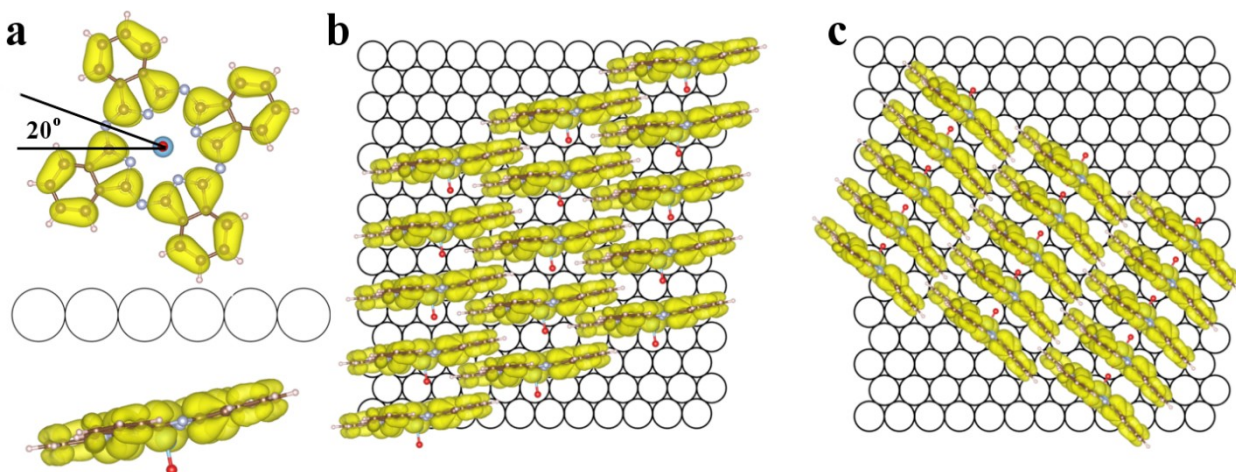
Figure 3. (a) Electron density of the highest occupied molecular orbital (HOMO) of titanyl phthalocyanine (TiOPc) viewed from directions perpendicular (upper image) and parallel (lower image) to the phthalocyanine ring. (b) Proposed packing arrangement of TiOPc molecules in hexagonal lattice on Au{111}. (c) Proposed packing arrangement of TiOPc molecules in rectangular lattice on Au{111}.

We investigated the photo-responses of molecules in the TiOPc hexagonal lattice using laser-assisted STM with 633 nm (3.5 mW) laser illumination. Consecutively obtained STM topographic images of the same region and simultaneously acquired spectroscopic images are shown in Figure 4. Figure 4b,d are spectroscopic images of in-phase lock-in signals with a reference frequency of 4.8 kHz created by a chopper wheel that was used to modulate

the evanescent sample illumination. The blue and green boxes, which highlight the same area in Figure 4a,b and Figure 4c,d, respectively, represent the unit cell of the hexagonal lattice; they contain a single TiOPc molecule. In Figure 4b,d, there are protrusions directly corresponding to the positions of TiOPc molecules in Figure 4a,c. In our experimental setup, the increase of tunneling current caused by laser-induced thermal expansion of the tunneling junction results in negative in-phase lock-in signals, as indicated by the color bar in Figure 4b,d. On the other hand, the protrusions in Figure 4b,d suggest that the corresponding positions have lower electron density during the illumination interval compared to the surrounding area.[25] Such distributions of lower photoelectron densities are attributed to the excitation of TiOPc molecules at 633 nm and relate to the differences in electron density between the exited state and ground state molecular orbitals.[42,45,47] Furthermore, as shown in Figure 4b,d, the probability for TiOPc molecules to be excited at 633 nm is different between molecules. For some TiOPc molecules, there are no corresponding protrusions in the spectroscopic images, indicating that those molecules have lower excitation probabilities. The local environment in this area can affect the distribution of the evanescent field and results in differences in excitation probabilities.
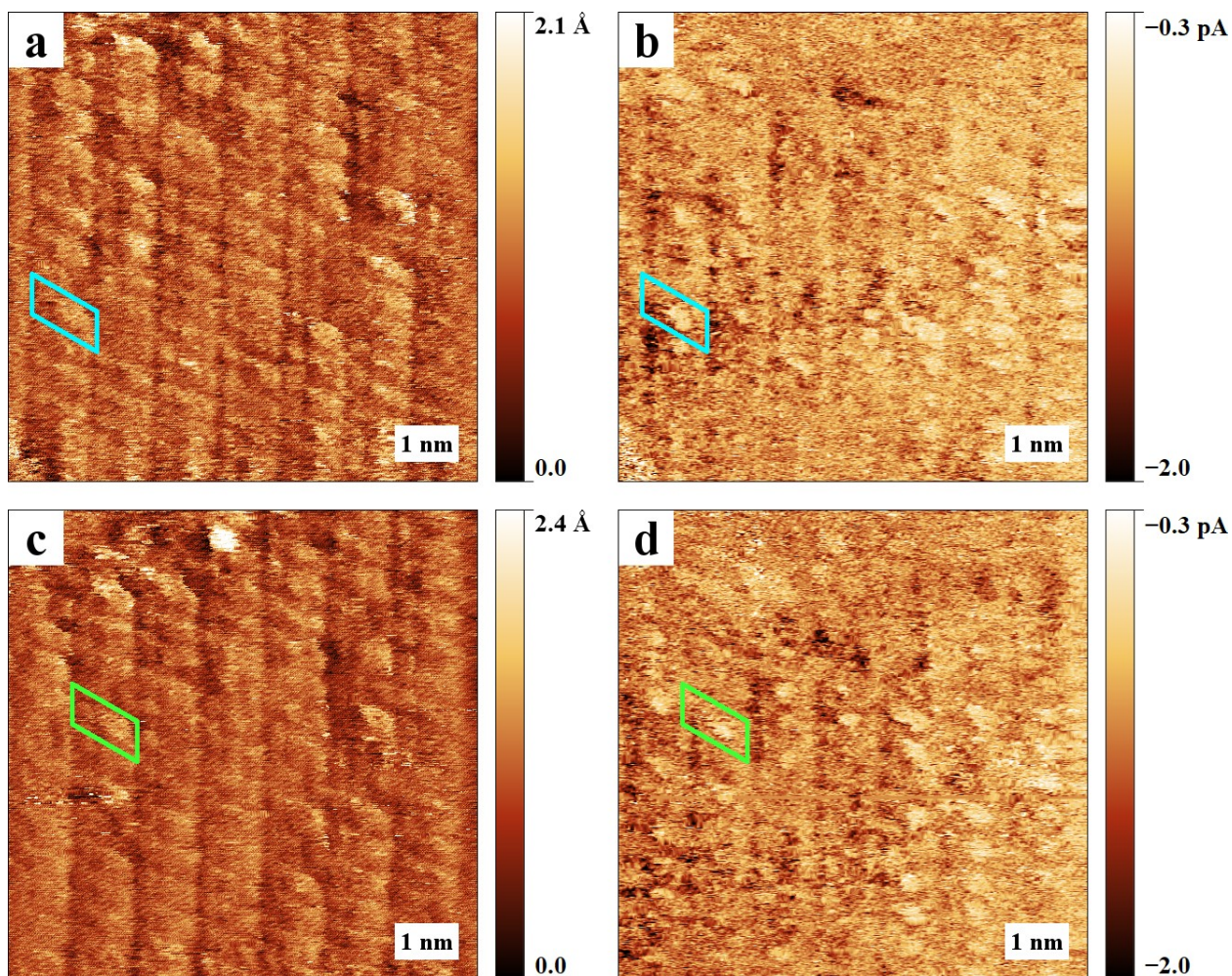
Figure 4. Consecutively collected scanning tunneling microscopy (STM) images under evanescent 633 nm laser (3.5 mW) illumination, showing titanyl phthalocyanine (TiOPc) monolayers (with a hexagonal lattice) on Au{111}. (a) Topographic and (b) spectroscopic images were simultaneously obtained. The blue boxes highlight the same area in corresponding images. (c) Topographic and (d) spectroscopic images were simultaneously obtained immediately after (a) and (b). The green boxes highlight the same area in corresponding images. All images were collected at a sample bias of −1.00 V and a tunneling current of 70.0 pA. All spectroscopic images were collected

phase sensitively with a reference frequency of 4.8 kHz created by a chopper wheel that was used to modulate the evanescent sample illumination.

We also excited the TiOPc molecules in the hexagonal lattice with 780 nm (7.7 mW) laser illumination. Figure 5a,b are topographic and simultaneously collected spectroscopic images obtained under evanescent 780 nm laser illumination at the same area as Figure 4. The yellow boxes in Figure 5 represent the shape of a unit cell of the hexagonal lattice and highlight the same area in corresponding images. From Figure 5b, we can see that under 780 nm illumination, the excitation of TiOPc molecules results in low photoelectron density in the local area, similar to 633 nm illumination. The distribution of photoelectrons in Figure 5b is not homogeneous across this area, indicating that this area may not be perfectly perpendicular to the polarization direction of the laser.
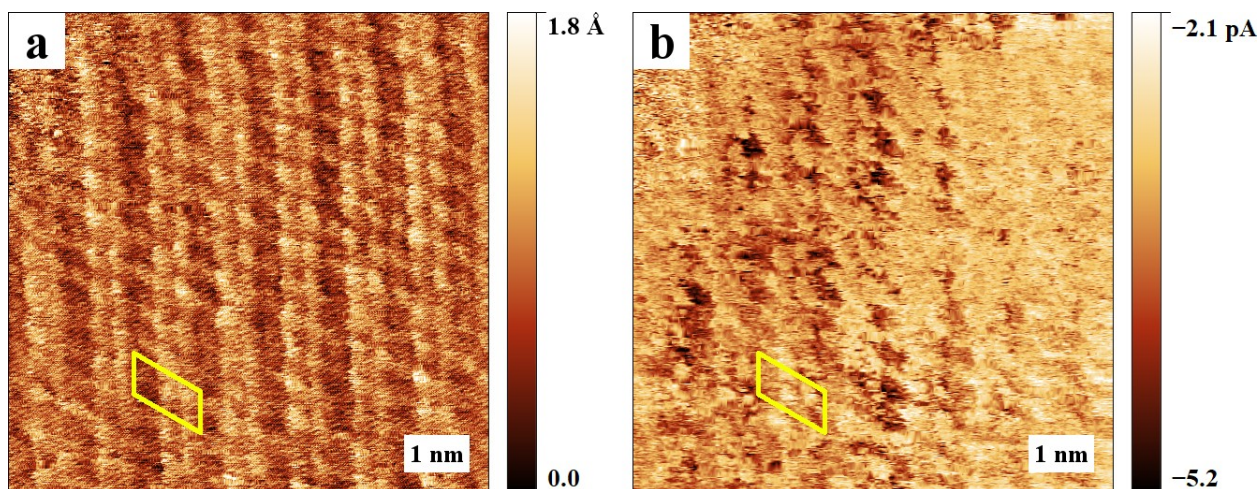

Figure 5. Scanning tunneling microscopy (STM) images collected under evanescent 780 nm laser (7.7 mW) illumination, showing titanyl phthalocyanine (TiOPc) monolayers (with a hexagonal lattice) on Au{111}.

(a) Topographic and (b) spectroscopic images were simultaneously obtained. The yellow boxes highlight the same area in corresponding images. All images were collected at a sample bias of -1.00 V and a tunneling current of 70.0 pA. Spectroscopic images were collected phase sensitively with a reference frequency of 4.8 kHz created by a chopper wheel that was used to modulate the evanescent sample illumination.

   In order to interpret the photoelectron distributions that we observed in Figures 4 and 5, we calculated the charge density differences between excited states and ground state molecular orbitals of TiOPc in hexagonal lattice. Charge density differences between the lowest unoccupied molecular orbital (LUMO) and HOMO of TiOPc are shown in Figure 6a,b. Charge density differences between LUMO+1 and HOMO of TiOPc are shown in Figure 6c,d. According to our calculations, the LUMO is doubly degenerate in the gas phase, but the energy band splits into two sub-bands in the hexagonal lattice, due to interactions between adjacent molecules (see supporting information). The excitation of TiOPc from HOMO to LUMO and LUMO+1 correspond to the Q band of TiOPc. In Figure 6, the yellow color represents increases in charge density when molecules are excited from the ground state to excited states, while the blue color represents decreases in charge density. We can see that there are decreases in charge density on the phenyl rings when TiOPc is excited from HOMO to LUMO or LUMO+1. This result is consistent with the spectroscopic images in Figure 4 and 5, and supports the conclusion that the laser-assisted STM characterizes the

distribution of photoelectrons in TiOPc hexagonal lattice. The slight differences between Figure 4b,d and Figure 5b may be due to the fact that TiOPc molecules are excited predominantly to the LUMO by the 780 nm light, and to the LUMO+1 by the 633 nm light. However, since our experiments were carried out at room temperature under ambient conditions, the topographic and spectroscopic images are likely to be convoluted, resulting in thermal smearing and shifts s of different the energy levels of the entire system,.[48-57] and Hence, the calculated results are not expected to match the experimental data precisely.
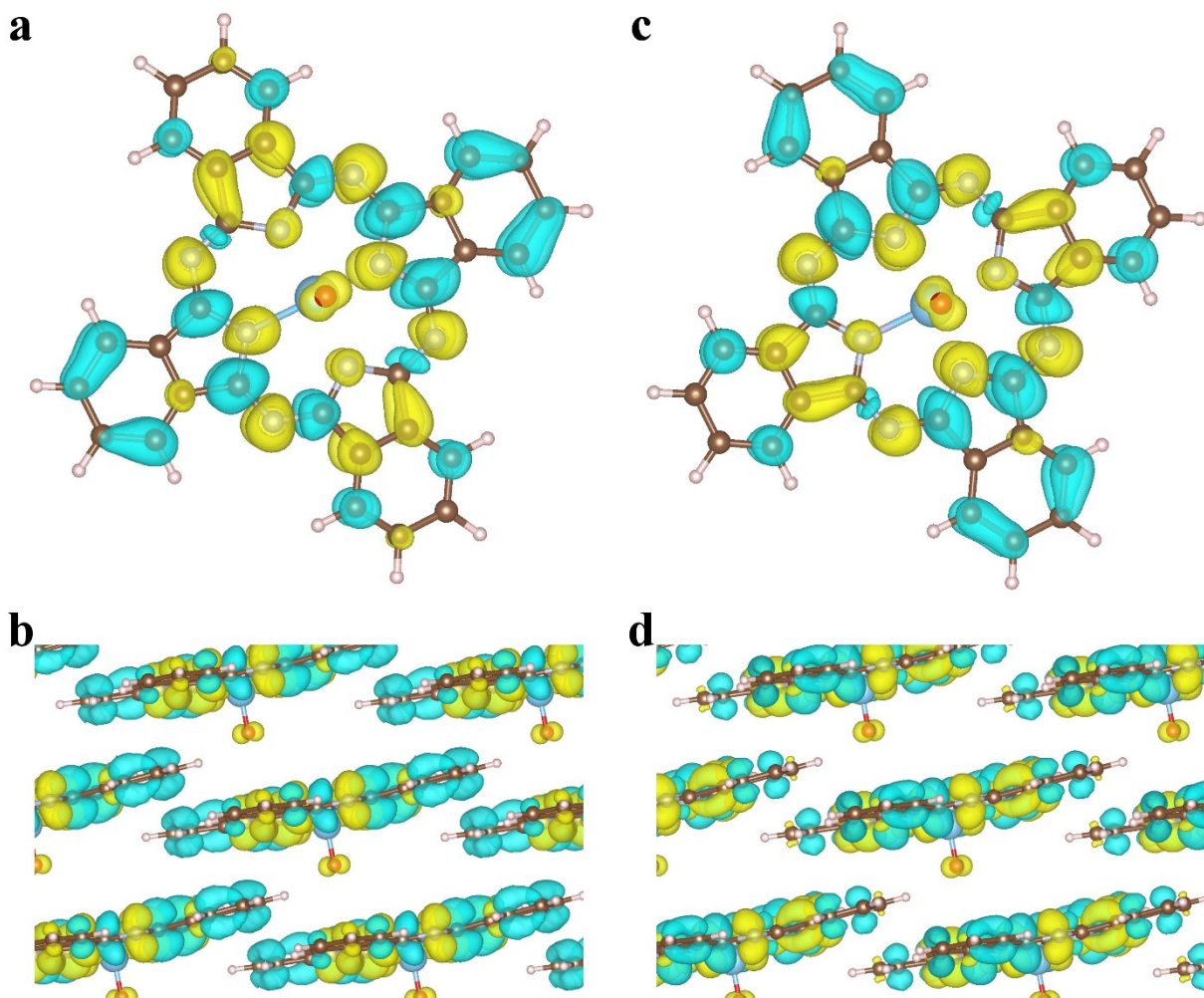
a

c

b

d

13

Figure 6. (a,b) Charge density differences between the lowest unoccupied molecular orbital (LUMO) and highest occupied molecular orbital (HOMO) of titanyl phthalocyanine (TiOPc) in hexagonal lattice. (c,d) Charge density differences between LUMO+1 and HOMO of TiOPc in the hexagonal lattice. The yellow color represents increases in charge density when molecules are excited from the ground state to excited states, while the blue color represents corresponding decreases in charge density.

In order to test the effects of thermal expansion and hot electron tunneling in the STM junction on the in-phase lock-in signal, we performed a control experiment by characterizing the hexagonal lattice under 405 nm laser (5 mW) illumination. Figure 7a,b are topographic and simultaneously collected spectroscopic images showing the hexagonal lattice obtained under 405 nm laser illumination. The pink boxes represent the shape of a unit cell for hexagonal lattice and highlight the same area in corresponding images. From Figure 7b we can see that TiOPc molecules correspond to more negative in-phase signals, which means that the corresponding positions have higher photoelectron densities than the surrounding area. Figure 7b is significantly different from the spectroscopic images collected under 633 or 780 nm laser illumination, and the increase of photoelectron density on top of the molecules does not match our DFT calculation results. Since TiOPc should not absorb 405 nm light as efficiently as 633 nm and 780 nm light,[12] we tentatively attribute such negative in-phase signals to the thermal expansion of the tunneling junction.

14
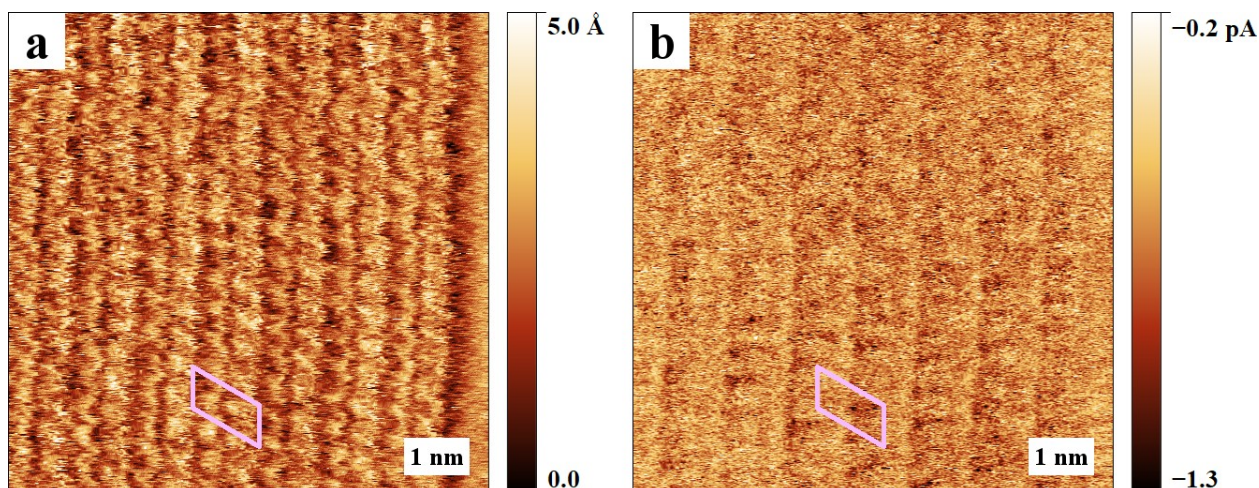
Figure 7. Scanning tunneling microscopy (STM) images collected under evanescent 405 nm laser (5 mW) illumination, showing titanyl phthalocyanine (TiOPc) monolayers (with a hexagonal lattice) on Au{111}. (a) Topographic and (b) spectroscopic images were simultaneously obtained. The pink boxes highlight the same area in corresponding images. All images were collected at a sample bias of −1.00 V and a tunneling current of 70.0 pA. Spectroscopic image was collected phase sensitively with a reference frequency of 4.8 kHz created by a chopper wheel that was used to modulate the evanescent sample illumination.

We also studied the photo-responses of molecules assembled into rectangular lattices using our laser-assisted STM with 633 nm and 780 nm laser illumination. Figure 8a,b shows simultaneously obtained topographic and spectroscopic images with 633 nm excitation. The white boxes represent the shape of a unit cell for rectangular lattice and highlight the same area in corresponding images. Figure 8c,d are simultaneously obtained topographic and spectroscopic images with 780 nm excitation. The black boxes represent

the shape of a unit cell for the rectangular lattice and highlight the same area in corresponding images. From Figure 8, we see that under both 633 nm and 780 nm excitation, TiOPc molecules correspond to higher photoelectron densities than the surrounding areas. This result indicates that the photo-responses of molecules in the rectangular lattices are different ~~than~~ from those in the hexagonal lattices. We calculated the charge density differences between excited state~~s~~ and ground state molecular orbitals of TiOPc, and the results are shown in Figure 9. By comparing Figure 9 with Figure 6, we can see that in the rectangular lattice, when TiOPc molecules are excited from HOMO to LUMO or LUMO+1, ~~there are more~~the charge density increases at the center of the macro ring more than ~~that for~~in the hexagonal lattice, but the general ~~distribution~~ change of charge density ~~changes~~ is similar to ~~those~~ ~~that for~~ in the hexagonal lattice. However, the photoelectron distribution in rectangular lattice does not match the theoretical prediction well, and that ~~which~~ indicates that TiOPc molecules may have low excitation probabilities in the rectangular lattice. The patterns we see in Figure 8 may have been caused by thermal expansion of the tunneling junction. Our data suggest that different packing arrangements of TiOPc in monolayers lead to different photo-responses. Our DFT calculations suggest that the energy gaps between HOMO and LUMO or LUMO+1 for TiOPc molecules in *hexagonal* lattices are ~~calculated to be~~ 1.5-2.0 eV (excluding the effects of the substrate, see supporting information), which matches the 633 nm and 780 nm photon energies. However, the energy

16

gaps between HOMO and LUMO or LUMO+1 for TiOPc molecules in *rectangular* lattices are calculated to be at or below 1.5 eV (excluding the effects of the substrate, see supporting information), indicating that 633 nm and 780 nm photons may not be absorbed strongly by TiOPc molecules packed in rectangular lattices.

We note that the conjugated backbones of TiOPc molecules are stacked more directly and densely in rectangular lattices than in hexagonal lattices. The π-π stacking between TiOPc molecules in rectangular lattices is rather large (4.0 Å) for strong coupling, but could nonetheless increase carrier mobility in the monolayers, reducing the observed local effects of the photoexcitation on single TiOPc molecules in laser-assisted STM measurements.[58-61] More detailed study is needed to correlate our results to the optoelectronic properties of TiOPc crystals and thin films.
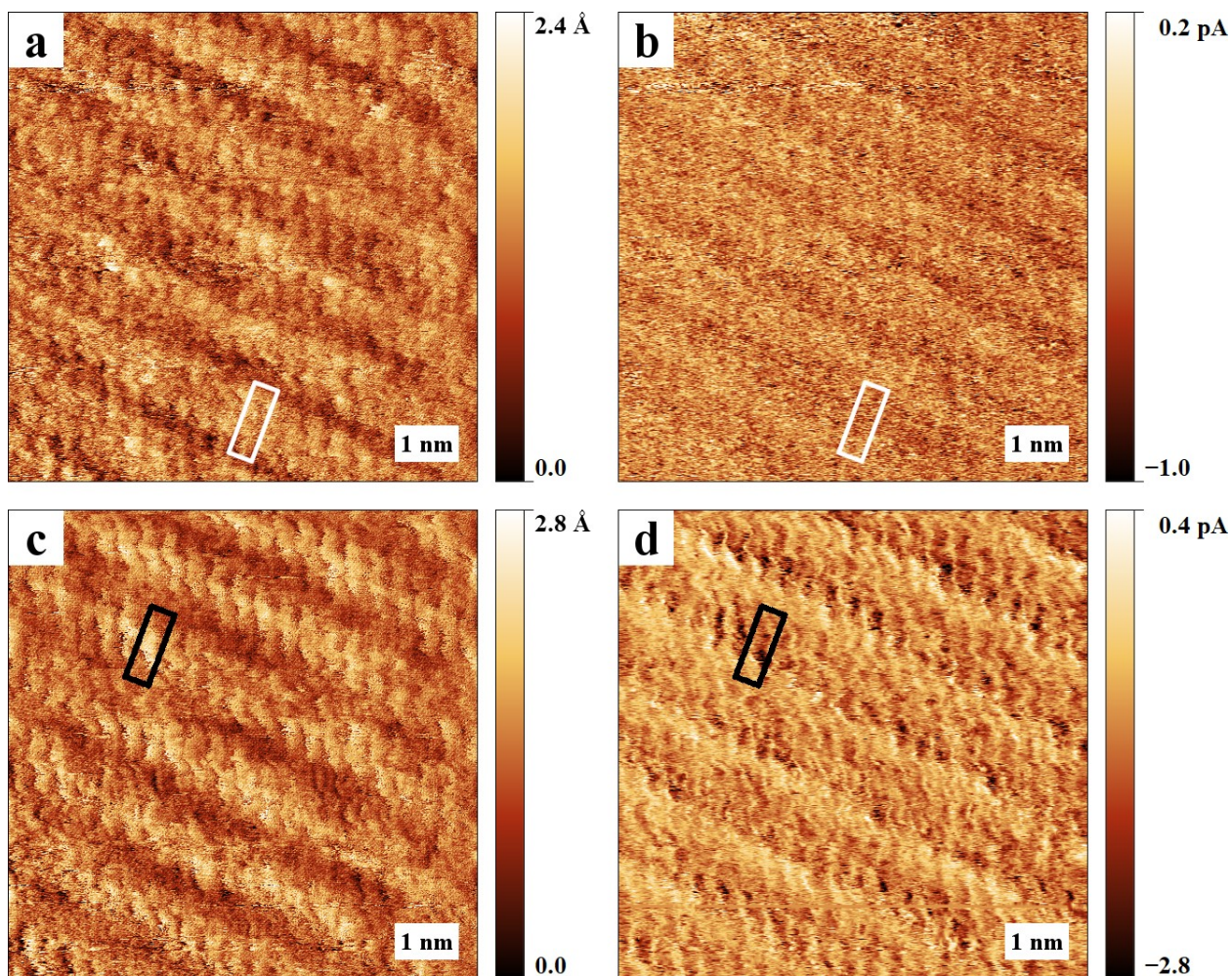
Figure 8. Scanning tunneling microscopy (STM) images collected under evanescent laser illumination, showing titanyl phthalocyanine (TiOPc) monolayers (with a rectangular lattice) on Au{111}. (a) Topographic and (b) spectroscopic images were simultaneously obtained when a 633 nm laser illuminated the sample evanescently. The white boxes highlight the same area in corresponding images. (c) Topographic and (d) spectroscopic images were simultaneously obtained when a 780 nm laser illuminated the sample evanescently. The black boxes highlight the same area in corresponding images. All images were collected at a sample bias of −1.00 V and a

tunneling current of 70.0 pA. All spectroscopic images were collected phase sensitively with a reference frequency of 4.8 kHz created by a chopper wheel that was used to modulate the evanescent sample illumination.
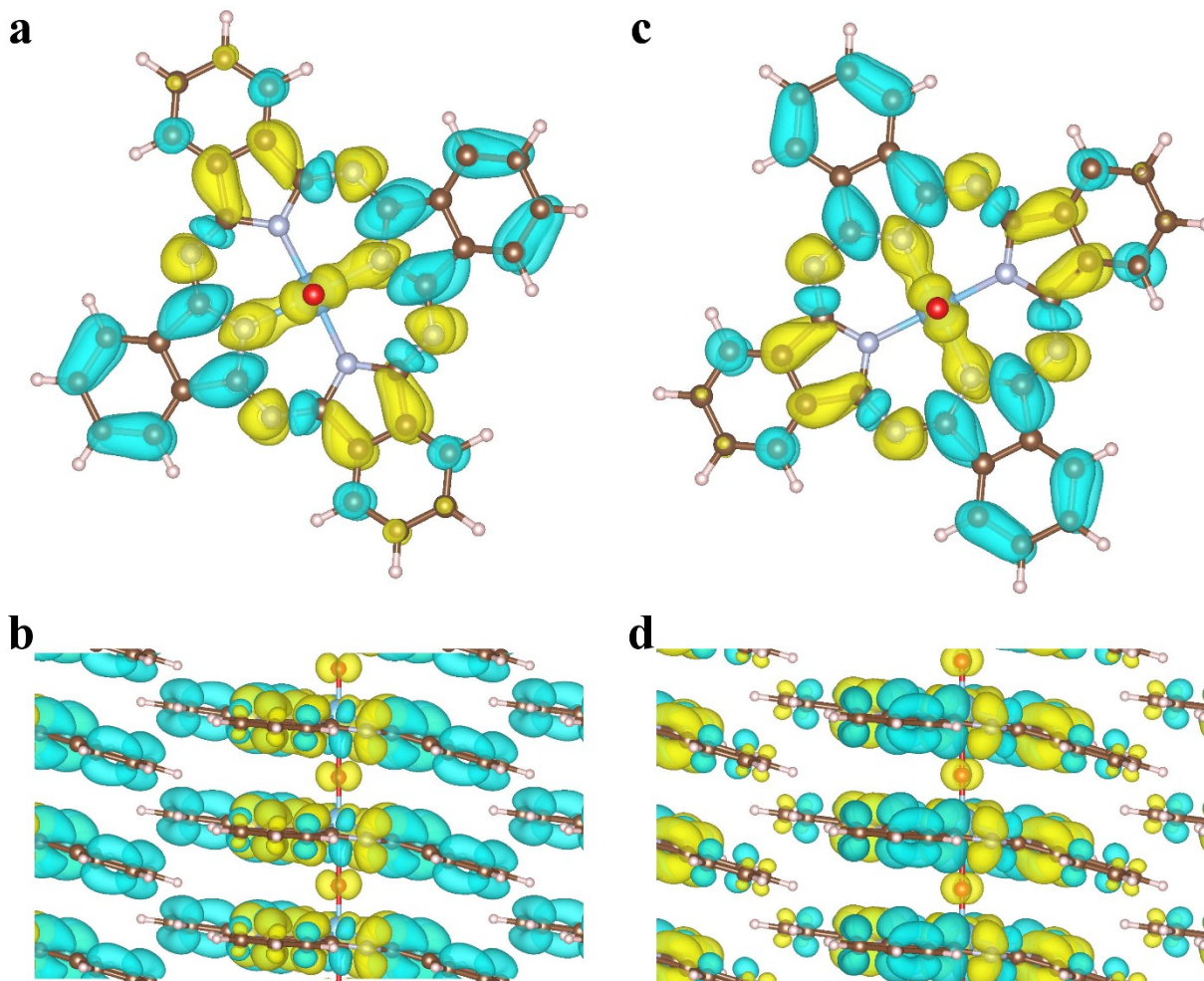
Figure 9. (a,b) Charge density differences between the lowest unoccupied molecular orbital (LUMO) and highest occupied molecular orbital (HOMO) of titanyl phthalocyanine (TiOPc) in a rectangular lattice. (c,d) Charge density differences between LUMO+1 and HOMO of TiOPc in a rectangular lattice. The yellow color represents increases in charge density when molecules are

excited from ground state to excited states, while the blue color represents corresponding decreases in charge density.

Conclusions and Prospects

Using laser-assisted STM, we have characterized the photo-responses of TiOPc molecules in two lattice structures we observed in solution deposited TiOPc monolayers on Au{111}. In hexagonal lattices, when TiOPc molecules are activated from HOMO to LUMO or LUMO+1 by 633 nm or 780 nm lasers, we observed lower photoelectron density on top of the molecules. Such results match the charge density differences between excited states and ground state molecular orbitals of TiOPc obtained by DFT calculations. The DFT predicted photo-responses of TiOPc molecules in rectangular lattices are similar to those in hexagonal lattices, but the photoelectron distributions that we observed experimentally in spectroscopic images are different from those predictions. Our data suggest that TiOPc molecules have lower excitation probabilities at 633 nm or 780 nm when organized in rectangular lattices than when in hexagonal lattices, and that the local environments can affect the absorption. By using the laser-assisted STM, we have elucidated photoelectron distributions with submolecular resolution that cannot otherwise be extracted. Our results provide insight into the importance of packing arrangements in photoexcitation and carrier generation efficiencies in bulk crystals, thin films, and smaller assemblies.

ASSOCIATED CONTENT

Supporting Information.

The supporting information is available free of charge.

The methodology followed for the preparation Au{111}/Al$_2$O$_3$(0001) substrates and monolayers and density functional theory calculation details.

AUTHOR INFORMATION

Corresponding Author

*Email: psw@cnsi.ucla.edu (P.S.W.).

*Email: ana@chem.ucla.edu (A.A.).

Author contributions

 The instrument and experiments were developed by S.W., N.C., N.W., K.B., and P.S.W. Density functional theory calculations were planned, performed, and analyzed by H.G., ~~P.S.,~~ and A.A. Experimental data were collected and analyzed by S.W., N.C., N.W., and K.B. The manuscript was written by S.W., N.C., H.G., and P.S.W. with assistance from all authors.

Notes

The authors declare no competing financial interest.

ORCID

Shenkai Wang: 0000-0002-2151-8664

Naihao Chiang: 0000-0003-3782-6546

Han Guo: 0000-0001-7695-9080

Natcha Wattanatorn: 0000-0001-5135-7761

Kristopher Barr: 0000-0002-8797-0012

Philippe Sautet: 0000-0002-8444-3348

Anastassia N. Alexandrova: 0000-0002-3003-1911

Paul S. Weiss: 0000-0001-5527-6248

ACKNOWLEDGMENTS

REFERENCES

(1) Brumbach, M.; Placencia, D.; Armstrong, N. R. Titanyl Phthalocyanine/ C_{60} Heterojunctions: Band-Edge Offsets and Photovoltaic Device Performance. *J. Phys. Chem. C* **2008,** *112*, 3142–3151.

(2) Placencia, D.; Wang, W.; Shallcross, R. C.; Nebesny, K. W.; Brumbach, M.; Armstrong, N. R. Organic Photovoltaic Cells Based On Solvent-Annealed, Textured Titanyl Phthalocyanine/C_{60} Heterojunctions. *Adv. Funct. Mater.* **2009,** *19*, 1913–1921.

(3) Placencia, D.; Wang, W.; Gantz, J.; Jenkins, J. L.; Armstrong, N. R. Highly Photoactive Titanyl Phthalocyanine Polymorphs as Textured Donor Layers in Organic Solar Cells. *J. Phys. Chem. C* **2011,** *115*, 18873–18884.

(4) Vasseur, K.; Rand, B. P.; Cheyns, D.; Temst, K.; Froyen, L.; Heremans, P. Correlating the Polymorphism of Titanyl Phthalocyanine Thin Films with Solar Cell Performance. *J. Phys. Chem. Lett.* **2012,** *3*, 2395–2400.

(5) Mayukh, M.; Macech, M. R.; Placencia, D.; Cao, Y.; Armstrong, N. R.; McGrath, D. V. Solution Processed Titanyl Phthalocyanines as Donors in Solar Cells: Photoresponse to 1000 nm. *ACS Appl. Mater. Interfaces* **2015,** *7*, 23912–23919.

(6) Sun, M.; Wang, S.; Xiao, Y.; Song, Z.; Li, X. Titanylphthalocyanine as Hole Transporting Material for Perovskite Solar Cells. *Journal of Energy Chemistry* **2015,** *24*, 756–761.

(7) Ramar, M.; Tyagi, P.; Suman, C. K.; Srivastava, R. Enhanced Carrier Transport in Tris(8-Hydroxyquinolinate) Aluminum by Titanyl Phthalocyanine Doping. *RSC Adv.* **2014,** *4*, 51256–51261.

(8) Li, L.; Tang, Q.; Li, H.; Yang, X.; Hu, W.; Song, Y.; Shuai, Z.; Xu, W.; Liu, Y.; Zhu, D. An Ultra Closely π-Stacked Organic Semiconductor for High Performance Field-Effect Transistors. *Adv. Mater.* **2007,** *19*, 2613–2617.

(9) Dong, S.; Bao, C.; Tian, H.; Yan, D.; Geng, Y.; Wang, F. ABAB-Symmetric Tetraalkyl Titanyl Phthalocyanines for Solution Processed Organic Field-Effect Transistors with Mobility Approaching 1 cm^2 V^{-1} s^{-1}. *Adv. Mater.* **2013,** *25*, 1165–1169.

(10) Park, J. H.; Movva, H. C. P.; Chagarov, E.; Sardashti, K.; Chou, H.; Kwak, I.; Hu, K.-T.; Fullerton-Shirey, S. K.; Choudhury, P.; Banerjee, S. K.; Kummel, A. C. In Situ Observation of Initial Stage in Dielectric Growth and Deposition of Ultrahigh Nucleation Density Dielectric on Two-Dimensional Surfaces. *Nano Lett.* **2015,** *15*, 6626–6633.

(11) Law, K. Y. Organic Photoconductive Materials: Recent Trends and Developments. *Chem. Rev.* **1993,** *93*, 449–486.

(12) Mizuguchi, J.; Rihs, G.; Karfunkel, H. R. Solid-State Spectra of Titanylphthalocyanine As Viewed from Molecular Distortion. *J. Phys. Chem.* **1995,** *99*, 16217–16227.

(13) Feenstra, R. M.; Stroscio, J. A.; Tersoff, J.; Fein, A. P. Atom-Selective Imaging of The GaAs(110) Surface. *Phys. Rev. Lett.* **1987,** *58*, 1192–1195.

(14) Reddick, R. C.; Warmack, R. J.; Ferrell, T. L. New Form of Scanning Optical Microscopy. *Phys. Rev. B* **1989,** *39*, 767–770.

(15) Hamers, R. J. Atomic-Resolution Surface Spectroscopy with the Scanning Tunneling Microscope. *Annu. Rev. Phys. Chem.* **1989,** *40*, 531–559.

(16) Meixner, A. J.; Bopp, M. A.; Tarrach, G. Direct Measurement of Standing Evanescent Waves with a Photon-Scanning Tunneling Microscope. *Appl. Opt.* **1994,** *33*, 7995–8000.

(17) Berndt, R.; Gaisch, R.; Schneider, W. D.; Gimzewski, J. K.; Reihl, B.; Schlittler, R. R.; Tschudy, M. Atomic Resolution in Photon Emission Induced by a Scanning Tunneling Microscope. *Phys. Rev. Lett.* **1995,** *74*, 102–105.

(18) Takahashi, S.; Fujimoto, T.; Kato, K.; Kojima, I. High Resolution Photon Scanning Tunneling Microscope. *Nanotechnology* **1997,** *8*, A54–A57.

(19) Stipe, B. C.; Rezaei, M. A.; Ho, W. Single-Molecule Vibrational Spectroscopy and Microscopy. *Science* **1998,** *280*, 1732–1735.

(20) McCarty, G. S.; Weiss, P. S. Scanning Probe Studies of Single Nanostructures. *Chem. Rev.* **1999,** *99*, 1983–1990.

(21) Donhauser, Z. J.; Mantooth, B. A.; Kelly, K. F.; Bumm, L. A.; Monnell, J. D.; Stapleton, J. J.; Price, D. W.; Rawlett, A. M.; Allara, D. L.; Tour, J. M.; Weiss, P. S. Conductance Switching in Single Molecules through Conformational Changes. *Science* **2001,** *292*, 2303–2307.

(22) Claridge, S. A.; Schwartz, J. J.; Weiss, P. S. Electrons, Photons, and Force: Quantitative Single-Molecule Measurements from Physics to Biology. *ACS Nano* **2011,** *5*, 693–729.

(23) Kim, M.; Hohman, J. N.; Cao, Y.; Houk, K. N.; Ma, H.; Jen, A. K. Y.; Weiss, P. S. Creating Favorable Geometries for Directing Organic Photoreactions in Alkanethiolate Monolayers. *Science* **2011,** *331*, 1312–1315.

(24) Bonnell, D. A.; Basov, D. N.; Bode, M.; Diebold, U.; Kalinin, S. V.; Madhavan, V.; Novotny, L.; Salmeron, M.; Schwarz, U. D.; Weiss, P. S. Imaging Physical Phenomena with Local Probes: From Electrons to Photons. *Rev. Mod. Phys.* **2012,** *84*, 1343–1381.

(25) Wang, S.; Wattanatorn, N.; Chiang, N.; Zhao, Y.; Kim, M.; Ma, H.; Jen, A. K. Y.; Weiss, P. S. Photoinduced Charge Transfer in Single-Molecule *p–n* Junctions. *J. Phys. Chem. Lett.* **2019,** *10*, 2175–2181.

(26) Kong, X.-H.; Yang, Y.-L.; Lei, S.-B.; Wang, C. On the Topography Multiplicity of Non-Planar Titanyl (IV) Phthalocyanine Molecules and the STM Imaging Mechanism. *Surf. Sci.* **2008,** *602*, 684–692.

(27) Wei, Y.; Robey, S. W.; Reutt-Robey, J. E. TiOPc Molecular Dislocation Networks as Nanotemplates for C_{60} Cluster Arrays. *J. Am. Chem. Soc.* **2009,** *131*, 12026–12027.

(28) Wei, Y. Y.; Reutt-Robey, J. E. Directed Organization of C_{70} Kagome Lattice by Titanyl Phthalocyanine Monolayer Template. *J. Am. Chem. Soc.* **2011,** *133*, 15232–15235.

(29) Wei, Y. Y.; Reutt-Robey, J. E. Molecular Interface Formation in Titanyl Phthalocyanine-C_{60} Monolayer Films. *J. Phys. Chem. C* **2012,** *116*, 23773–23778.

(30) Liu, X.; Wei, Y.; Reutt-Robey, J. E.; Robey, S. W. Dipole–Dipole Interactions in TiOPc Adlayers on Ag. *J. Phys. Chem. C* **2014,** *118*, 3523–3532.

(31) Park, J. H.; Fathipour, S.; Kwak, I.; Sardashti, K.; Ahles, C. F.; Wolf, S. F.; Edmonds, M.; Vishwanath, S.; Xing, H. G.; Fullerton-Shirey, S. K.; Seabaugh, A.; Kummel, A. C. Atomic Layer Deposition of Al_2O_3 on WSe_2 Functionalized by Titanyl Phthalocyanine. *ACS Nano* **2016,** *10*, 6888–6896.

(32) Zhao, W.; Zhu, H.; Song, H.; Liu, J.; Chen, Q.; Wang, Y.; Wu, K. Adsorption and Assembly of Photoelectronic TiOPc Molecules on Coinage Metal Surfaces. *J. Phys. Chem. C* **2018,** *122*, 7695–7701.

(33) Vigoureux, J. M.; Girard, C.; Courjon, D. General Principles of Scanning Tunneling Optical Microscopy. *Opt. Lett.* **1989,** *14*, 1039–1041.

(34) Reddick, R. C.; Warmack, R. J.; Chilcott, D. W.; Sharp, S. L.; Ferrell, T. L. Photon Scanning Tunneling Microscopy. *Rev. Sci. Instrum.* **1990,** *61*, 3669–3677.

(35) Jiang, S.; Tomita, N.; Ohsawa, H.; Ohtsu, M. A Photon Scanning Tunneling Microscope Using an AlGaAs Laser. *Jpn. J. Appl. Phys.* **1991,** *30*, 2107–2111.

(36) Dawson, P.; de Fornel, F.; Goudonnet, J. P. Imaging of Surface Plasmon Propagation and Edge Interaction Using a Photon Scanning Tunneling Microscope. *Phys. Rev. Lett.* **1994,** *72*, 2927–2930.

(37) Feldstein, M. J.; Vohringer, P.; Wang, W.; Scherer, N. F. Femtosecond Optical Spectroscopy and Scanning Probe Microscopy. *J. Phys. Chem.* **1996,** *100*, 4739–4748.

(38) Ballard, J. B.; Carmichael, E. S.; Shi, D.; Lyding, J. W.; Gruebele, M. Laser Absorption Scanning Tunneling Microscopy of Carbon Nanotubes. *Nano Lett.* **2006,** *6*, 45–49.

(39) Shigekawa, H.; Yoshida, S.; Takeuchi, O.; Aoyama, M.; Terada, Y.; Kondo, H.; Oigawa, H. Nanoscale Dynamics Probed by Laser-Combined Scanning Tunneling Microscopy. *Thin Solid Films* **2008,** *516*, 2348–2357.

(40) Wu, S. W.; Ho, W. Two-Photon-Induced Hot-Electron Transfer to a Single Molecule in a Scanning Tunneling Microscope. *Phys. Rev. B* **2010,** *82*, 085444.

(41) Atkin, J. M.; Berweger, S.; Jones, A. C.; Raschke, M. B. Nano-Optical Imaging and Spectroscopy of Order, Phases, and Domains in Complex Solids. *Adv. Phys.* **2012,** *61*, 745–842.

(42) Nienhaus, L.; Goings, J. J.; Nguyen, D.; Wieghold, S.; Lyding, J. W.; Li, X. S.; Gruebele, M. Imaging Excited Orbitals of Quantum Dots: Experiment and Electronic Structure Theory. *J. Am. Chem. Soc.* **2015,** *137*, 14743–14750.

(43) Nienhaus, L.; Wieghold, S.; Nguyen, D.; Lyding, J. W.; Scott, G. E.; Gruebele, M. Optoelectronic Switching of a Carbon Nanotube Chiral Junction Imaged with Nanometer Spatial Resolution. *ACS Nano* **2015,** *9*, 10563–10570.

(44) Cocker, T. L.; Peller, D.; Yu, P.; Repp, J.; Huber, R. Tracking the Ultrafast Motion of a Single Molecule by Femtosecond Orbital Imaging. *Nature* **2016,** *539*, 263–267.

(45) Nguyen, D.; Nguyen, H. A.; Lyding, J. W.; Gruebele, M. Imaging and Manipulating Energy Transfer Among Quantum Dots at Individual Dot Resolution. *ACS Nano* **2017,** *11*, 6328–6335.

(46) Mazur, U.; Leonetti, M.; English, W. A.; Hipps, K. W. Spontaneous Solution-Phase Redox Deposition of a Dense Cobalt(II) Phthalocyanine Monolayer on Gold. *The Journal of Physical Chemistry B* **2004,** *108*, 17003–17006.

(47) Nguyen, D.; Goings, J. J.; Nguyen, H. A.; Lyding, J.; Li, X. S.; Gruebele, M. Orientation-Dependent Imaging of Electronically Excited Quantum Dots. *J. Chem. Phys.* **2018,** *148*, 064701.

(48) Eigler, D. M.; Weiss, P. S.; Schweizer, E. K.; Lang, N. D. Imaging Xe with a Low-Temperature Scanning Tunneling Microscope. *Phys. Rev. Lett.* **1991,** *66*, 1189–1192.

(49) Sautet, P.; Joachim, C. Interpretation of STM Images: Copper-Phthalocyanine on Copper. *Surf. Sci.* **1992,** *271*, 387–394.

(50) Chavy, C.; Joachim, C.; Altibelli, A. Interpretation of STM Images: C_{60} on the Gold (110) Surface. *Chem. Phys. Lett.* **1993,** *214*, 569–575.

(51) Vion, D.; Orfila, P. F.; Joyez, P.; Esteve, D.; Devoret, M. H. Miniature Electrical Filters for Single Electron Devices. *J. Appl. Phys.* **1995,** *77*, 2519–2524.

(52) Bumm, L. A.; Arnold, J. J.; Dunbar, T. D.; Allara, D. L.; Weiss, P. S. Electron Transfer through Organic Molecules. *J. Phys. Chem. B* **1999,** *103*, 8122–8127.

(53) Pascual, J. I.; Gómez-Herrero, J.; Rogero, C.; Baró, A. M.; Sánchez-Portal, D.; Artacho, E.; Ordejón, P.; Soler, J. M. Seeing Molecular Orbitals. *Chem. Phys. Lett.* **2000,** *321*, 78–82.

(54) Pascual, J. I.; Jackiw, J. J.; Song, Z.; Weiss, P. S.; Conrad, H.; Rust, H. P. Adsorbate-Substrate Vibrational Modes of Benzene on Ag(110) Resolved with Scanning Tunneling Spectroscopy. *Phys. Rev. Lett.* **2001,** *86*, 1050–1053.

(55) Villagomez, C. J.; Zambelli, T.; Gauthier, S.; Gourdon, A.; Stojkovic, S.; Joachim, C. STM Images of a Large Organic Molecule Adsorbed on a Bare Metal Substrate or on a Thin Insulating Layer: Visualization of HOMO and LUMO. *Surf. Sci.* **2009,** *603*, 1526–1532.

(56) Pham, B. Q.; Gordon, M. S. Can Orbitals Really Be Observed in Scanning Tunneling Microscopy Experiments? *J. Phys. Chem. A* **2017,** *121*, 4851–4852.

(57) Puschnig, P.; Boese, A. D.; Willenbockel, M.; Meyer, M.; Lüftner, D.; Reinisch, E. M.; Ules, T.; Koller, G.; Soubatch, S.; Ramsey, M. G.; Tautz, F. S. Energy Ordering of Molecular Orbitals. *J. Phys. Chem. Lett.* **2017,** *8*, 208–213.

(58) Egbe, D. A. M.; Türk, S.; Rathgeber, S.; Kühnlenz, F.; Jadhav, R.; Wild, A.; Birckner, E.; Adam, G.; Pivrikas, A.; Cimrova, V.; Knör, G.; Sariciftci, N. S.; Hoppe, H. Anthracene Based Conjugated Polymers: Correlation between π−π-Stacking Ability, Photophysical Properties, Charge Carrier Mobility, and Photovoltaic Performance. *Macromolecules* **2010,** *43*, 1261–1269.

(59) Giri, G.; Verploegen, E.; Mannsfeld, S. C. B.; Atahan-Evrenk, S.; Kim, D. H.; Lee, S. Y.; Becerril, H. A.; Aspuru-Guzik, A.; Toney, M. F.; Bao, Z. Tuning Charge Transport in Solution-Sheared Organic Semiconductors Using Lattice Strain. *Nature* **2011,** *480*, 504–508.

(60) Okamoto, T.; Nakahara, K.; Saeki, A.; Seki, S.; Oh, J. H.; Akkerman, H. B.; Bao, Z.; Matsuo, Y. Aryl−Perfluoroaryl Substituted Tetracene: Induction of Face-to-Face π−π Stacking and Enhancement of Charge Carrier Properties. *Chem. Mater.* **2011,** *23*, 1646–1649.

(61) Mei, J.; Diao, Y.; Appleton, A. L.; Fang, L.; Bao, Z. Integrated Materials Design of Organic Semiconductors for Field-Effect Transistors. *J. Am. Chem. Soc.* **2013,** *135*, 6724–6746.